Formation of annealing twins during primary recrystallization of two low stacking fault energy Ni-based alloys

W Wang, S Lartigue-Korinek, F Brisset, A L Helbert, J Bourgon, T Baudin

Formation of annealing twins during primary recrystallization of two low stacking fault energy Ni-based alloys

W. Wang[1*], S. Lartigue-Korinek[2a], F. Brisset[1b], A. L. Helbert[1c], J. Bourgon[2d], T. Baudin[1e]

[1]*Université Paris-Sud, ICMMO, UMR CNRS 8182, 91405 Orsay Cedex, France*

[2]*Institut de Chimie et des Matériaux Paris Est, MCMC, UMR CNRS 7182, 94320 Thiais, France*

Corresponding Author: wei.wang@u-psud.fr, Université Paris-Sud, ICMMO, UMR CNRS 8182, bât. 410, 91405 Orsay Cedex, France. Tel: + (33) 1 69 15 47 89, Fax: + (33) 1 69 15 47 97.

a lartigue@icmpe.cnrs.fr

b francois.brisset@u-psud.fr

c anne-laure.helbert@u-psud.fr

d bourgon@icmpe.cnrs.fr

e thierry.baudin@u-psud.fr

Abstract.

First stages of recrystallization are analyzed in low stacking fault energy nickel alloys cold rolled and subsequently annealed at 700°C for 6 minutes. These alloys are envisaged as candidate materials for the heat exchanger of VHTR (Very High Temperature Reactor) that works at 1000°C. First recrystallized grains show evidence of extensive twinning that is studied by Transmission Electron Microscopy. Specific twinning features such as five-fold twin and microtwins bordered by partial dislocations are revealed. Twin density increases with increasing amounts of prior deformation before annealing. The local crystal orientations are determined at a nanometer scale. It is shown directly that when twinning occurs, the recrystallized area beyond the twin has a lower stored deformation energy. Thus recrystallization and the associate twinning induce a decrease in the total stored deformation energy.

Keywords: *Nickel alloy, Twinning, Stored energy, TEM, EBSD*

1 Introduction

Ni based alloys with low stacking fault energy (SFE) display extensive twinning from the start of primary recrystallization. Twinning occurs in recrystallized grains behind migrating grain boundaries (GBs). Until now, most studies concerned the mechanisms of twinning during grain growth. But, very few is known on the occurrence of twinning at the very beginning of primary recrystallization. The main driving forces for GB migration are supposed to be different during primary recrystallization and grain growth, however twinning events are related in both cases to GB migration and require a driving force. Twins are connected to migrating GBs and the mechanism of twinning could be similar.

With respect to the formation of twinning during grain growth, Fullman and Fisher in 1951 [1] proposed that twins are formed near triple junctions of moving grain boundaries, the driving force being an overall decrease in interfacial energy. Twinning was then explained by a stacking error or a ‘growth accident’ occurring at

GBs or triple junctions that induces the splitting and subsequent migration of a GB segment, leaving behind two coherent twin boundaries [2]. Following this approach, Gleiter [3] proposed an atomistic model that involves a two dimensional nucleation on close packed planes of the growing grain just at the point where the GB is parallel to {111} planes of the growing grain. A quite different nucleation process was also proposed which involves a direct stacking fault emission at GB ledges producing two twin segments, a coherent twin and an incoherent one; the further migration of the incoherent twin may induce a twinned region [4]. In all these works, the driving force is a reduction in the overall interfacial energy. If recovery is not completed, a decrease in dislocation density is also evoked [4]. But, a limitation of these models is that the initial orientation relationship between two grains must be close to a twin orientation, or the newly formed GB must have a low energy, two conditions that seem difficult to realize. Both experiments and simulation find that most GBs have a high interfacial energy [5-6].

In an attempt to interpret all the features of annealing twins, a microscopic model proposes that annealing twins are produced with the formation of a partial Shockley loop at the {111} ledges formed in migrating GBs [7-8]. The theory is based on the idea that annealing and deformation twins are crystallographically identical. The higher the GB velocity, the higher the probability for twin nucleation. Twin emission by migrating GBs during recrystallization had been evidenced previously, the twin nucleus being a stacking fault or a thin packet of stacking faults, bordered by Shockley partial dislocations [9]. The tips of annealing twins could be described as arrays of Shockley partial dislocations, but were fundamentally different from deformation twins in that for the tips of annealing twins the partials can be equally distributed amongst all three partials, allowing for a blocky tip and strain relaxation since the net burgers vector can cancel.

The emission of partial dislocations has also been found by Molecular Dynamics (MD) to interpret twinning during grain growth in nanocrystalline copper [10]. However in the recent experiments on twin characteristics in nanocrystalline thin films, the authors exclude such a mechanism, arguing that the required internal stresses are too high [11].

In recrystallized materials that have undergone a high deformation level before annealing, some twin characteristics are worth noticing. From a mesoscopic point of view it was found in nickel that the density of annealing twins decreases with the grain size, whatever time and temperature, and depends on the driving force for GB migration [12]. The twin number/grain size dependence applied well with other low SFE materials such as copper alloys [12]. The weak dependence of twinning with temperature is consistent with the model based on dislocation emission [7]. In the particular case of low temperature annealing where recovery is predominant, twinning started when the grain growth or GB migration was restrained, as revealed in copper and nickel by in situ experiments [13-14]. Thus twining is tightly linked to the further onset of grain boundary migration. The studies during early stage of recrystallization revealed also that twinning promotes the nucleation process in two types of stainless steel and α-brass [15].

The occurrence of twinning during recrystallization and especially the role of the deformation level prior to the heat

treatment is worth studying as it could shed light on twinning phenomena, in particular the relationship between onset of twinning and stored energy. Our previous works on recrystallization in nickel alloys have shown that the number of Σ3 GBs increased with the stored energy resulting from a prior deformation before annealing [16]. A similar result was found in an austenitic stainless steel [17]. Moreover, the twin density increases during recrystallization and decreases during grain growth in pure nickel, and twin formation was only observed for GBs migrating into deformed regions [18].

The present paper analyzes the twin formation in two nickel-based alloys by putting the focus on the features occurring in the very first stages of recrystallization. These materials have much lower stacking fault energy γ_{SFE} (between 4 and 10 mJ/m^2) than pure nickel and copper alloys. Twinning features are investigated by Transmission Electron Microscopy (TEM). The originality of this study is to determine the local orientations at a nanometer scale, allowing establishing a relationship between twinning and intragranular stored energy. Twinning mechanisms during first stages of recrystallization are finally discussed.

2 Experimental details

Two nickel alloys were produced by hot forging. One is monophasic (sample A), the other contains W particles as a second phase (sample B). Their chemical compositions are presented in table 1. For both materials, sheets of 1 cm thickness were cut from the ingots, cold-rolled with 90% reduction and annealed at 900°C for 3 hours in argon atmosphere. Under these treatments, a homogenous distribution of the chemical composition was obtained, together with a homogenous microstructure and an almost isotropic texture. The mean grain size is about 17 µm for sample A and 8 µm for sample B in these conditions. Afterwards, the sheets were cold-rolled with different reduction level and the corresponding true strains are shown in table 2. Then they were annealed at 900°C during 4 min so as to obtain a complete recrystallization [16]. Moreover, for each material, the one deformed with 80% reduction was annealed during 6 min at 700°C so as to develop the first stage of recrystallization.

The microstructure after annealing was studied on the transverse plane (Rolling Direction RD - Normal Direction ND) with a TSL/EDAX Electron BackScatter Diffraction (EBSD) system installed on a Field Emission Gun Scanning Electron Microscope (FEG-SEM). The analyzed maps were based on hexagonal grid. Those after complete recrystallization (900°C) were analyzed for an area of 150 x 350 µm^2 with 100 nm as step size, and the densities of Σ3 and Σ9 GBs were analyzed statistically. Those after partial recrystallization (700°C) were studied with 50 nm as step size. All samples were prepared by mechanical polishing up to 1/4 µm diamond polishing and finally polished using a colloidal silica suspension (OPS) with particle size of about 0.04 micron.

In the samples that underwent first stage of recrystallization, the recrystallized areas were studied with a JEOL 2000EX TEM. Thin foil preparation is described in [19]. The distribution of misorientations was determined thanks to an Automatic Crystal Orientation Mapping (ACOM) system in a FEI Tecnai F20 TEM (spot size 8, camera length 7.1 cm, condenser aperture 10 µm,

Table 1 chemical composition of the studied nickel alloys

Wt.%	Ni	Cr	W	Si	Mn	Mo	Al	Ti
Sample A	68.8	5.7	25.2	0.065	0.086	0.07	0.08	0.13
Sample B	60.7	19.6	19.9	0.075	0.08	0.05	0.1	0.14

gun lens 6, extraction voltage at 4.3 kV, resulting probe size 1.2 nm). An ASTAR system was used for ACOM diffraction data acquisition [20]. The analyzed map step was 10 nm based on a square grid. The crystallographic orientations are obtained through image matching between the experimental diffraction pattern and calculated templates with an orientation step of one degree between two successive templates.

Table 2 True strain prior to annealing

Rolling reduction	40%	60%	80%
True strain	0.59	1.06	1.86

EBSD and ACOM data were processed by using the OIM^{TM} software. For each point of scanned area, the retained images describe an Image Quality (IQ) that depends on the distortion of crystal lattice. This parameter is useful for the embodiment of the strain distribution in the material. Moreover, for each pixel, the Inverse Pole Figure (IPF) shows the crystal direction that is aligned with the chosen direction of reference (IPF [100], [010] and [001] mean respectively the rolling direction, the transverse direction and the normal direction of sample that is the reference direction). Then the pixels are colored according to the code defined in the unit triangle (for example, the red color in IPF [001] means the crystal direction <001> of the pixel is parallel to the normal direction of the sample).

3 Results

3.1 Recrystallization mechanisms

Fig. 1 shows the microstructure of two materials after a 6 min annealing at 700°C. New grains can be found within the surrounding deformed environment. The recrystallization seems to be faster in sample B than in A, with upper number of new grains. A statistical study with the help of microharness analyses shows that the recrystallization fraction is 6% and 8% in sample A and B respectively. The formation of Σ3 GBs was observed inside these new grains for both materials. The little recrystallization advantage in sample B should be related to the presence of second phase. Indeed, during the cold deformation, second phase particles act as obstacles to dislocation slip. This induces the formation of local deformation around particles, which become favorable sites for nucleation of recrystallized grains during subsequent annealing. This recrystallization mechanism is called particle stimulated nucleation (PSN) [21].

Figs. 2a-b show the presence of a bulge in sample A after the same annealing process. The crystal close to the bulge may be seen as a small recrystallized grain which could have been produced according to the Strain Induced Boundary Migration (SIBM) mechanism. This mechanism, firstly observed in 1950 [22], is related to the migration of a pre-existing grain boundary, leaving a dislocation free area behind it [21]. A similar microstructural feature occurs in a Fe-36%Ni alloy [23]. Such a bulge is also proposed to occur by the stress-driven GB

motion during the deformation [24]. In any case the stored energy behind the bulge is very small which favors its growth towards the adjacent area with a higher stored energy.

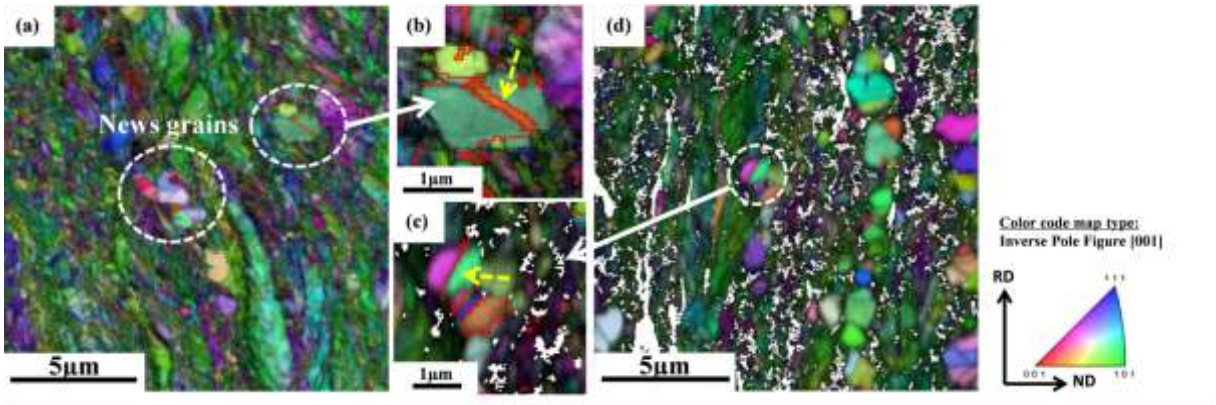

Fig. 1 Images issued from EBSD analyses (FEG-SEM) showing IQ + IPF [001] map (a) sample A. Regions with new recrystallized grains are circled. One of them is enlarged in (b); (c) and (d) sample B after annealing at 700°C for 6 min. GBs in red correspond to Σ3(yellow arrow). The white areas in (c) and (d) are the clusters of second phase W

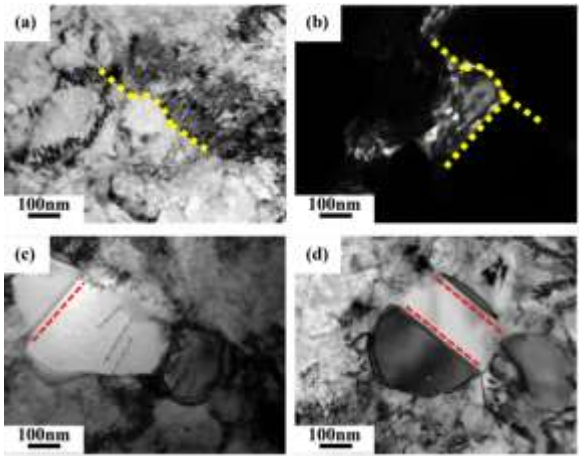

Fig. 2 TEM images after annealing at 700°C for 6 min of sample A. (a) bright-field image and (b) dark-field image indicating bulging of a GB; (c) and (d) bright-field images showing formation of twins inside the new grains during recrystallization. The red and yellow lines show the Σ3 and the pre-exiting grain boundaries, respectively

Figs. 2c-d reveal the presence of annealing twins inside new grains. Some isolated dislocations lie within the grain and are parallel to the twin boundaries. The twin boundary traces are thus aligned with one of the {111} planes (slip dislocation planes) of the recrystallized grains. This reveals that coherent twins are formed at the very beginning of the primary recrystallization. A microtwin parallel to a {111} plane presents dislocations at its extremity (Fig. 3a). In the 2 beam conditions of fig. 3b, the twin is not visible and the dislocations show a symmetrical contrast characteristic of $g.b = 0$, in agreement with a Burgers vector of twinning dislocations equal to 1/6 [2-1-1].

The local microstructure of sample B after annealing is shown in figure 4. The new grains are either close to or distant from the W particles (Fig. 4a). SIBM and PSN mechanism have been both activated. The simultaneous presence of two recrystallization mechanisms can explain the little advantage of recrystallization at the beginning of annealing in sample B.

Multiple twinning occurs within new grains. (Figs. 4b-d). As many twins are formed from the same parent grain adjacent twins can meet each other and form Σ9 boundary at the triple junction (yellow line in Fig. 4c). This phenomenon has been largely studied during grain boundary

engineering, where a large number of $\Sigma 3^n$ ($n \geq 1$) GBs is related to the association and dissociation of GBs [25].

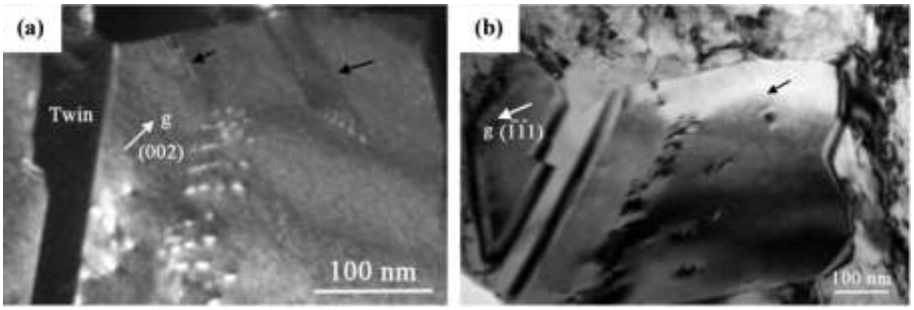

Fig. 3 TEM images after annealing at 700°C for 6 min of sample A. (a) Dark field image (2-beams conditions *g*=(002)) showing a twin and two microtwins (arrowed) inside a recrystallized grain. On the bright field image (b), the arrowed microtwin is out of contrast, but the dislocations at its extremity show a symmetrical contrast

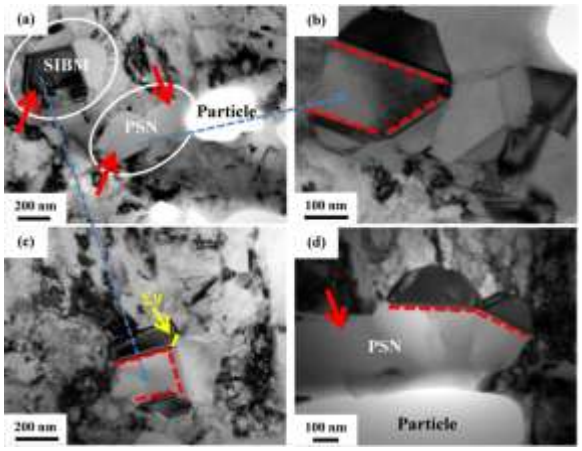

Fig. 4 Bright field TEM images of sample B after annealing at 700°C for 6 min. (a) Bright-field image showing recrystallized areas associated with SIBM and PSN. The particles have been dissolved during thinning; (b)-(d) multiple twins occur inside new grains. The red and yellow lines show the Σ3 and Σ9 boundaries, respectively

3.2 Annealing twin

The Figs. 5 and 6 show ACOM maps for samples A and B, respectively. The red lines are the GBs which have the Σ3 misorientation relationship. In Fig. 5c, the blue lines show the 4 {111} crystal plane traces on each side of the Σ3 boundary and the dotted ones show the common plane. The mean trend line of Σ3 is shown with orange dotted line. Thus the Σ3 boundary is parallel to a common {111} plane and corresponds to a coherent one, as most twins indicated by red lines in the recrystallized grains of Figs. 5a and 6a. This type of twin boundaries is always straight.

In addition, incoherent twin boundaries Σ3incoh are also present and an example is indicated with yellow line (boundary 2) in Fig. 5d. This twin part is located between the boundaries 1 and 3 that are coherent twins. The formation of this incoherent twin should be the outcome of the different formation times and/or locations of the two coherent twins. A similar feature is found by MD simulations [10].

The incoherent twin boundary is conventionally defined by its plane that is close to a common {112} plane. This definition is then extended to all boundaries whose plane is different from a common {111} plane [25]. In Fig. 5d, the Σ3incoh boundary 2 is deviated from the {112} and {111} orientations. However, it could be faceted at the atomic level.

The grain in the center of Fig. 5a shows evidence of five-fold twinning. This feature

is rather surprising as it usually occurs in nanoparticles or nanocrystalline materials. Observed for the first time in 1959 [26], five-fold twins are described as five crystals twin-related to each other, the five twin planes sharing a common <110> direction. The apex angle between twins should be 72° (360°/5). As the angle between twins in a perfect CFC lattice is 70.53°, a disclination with an angle close to 7.5° must occur. Such a defect is usually accommodated elastically or with the formation of sub-boundaries [27-28]. In the present case, a sub-boundary is present close to a twin and starts from the center of the five-fold twin as shown in Fig. 5b.

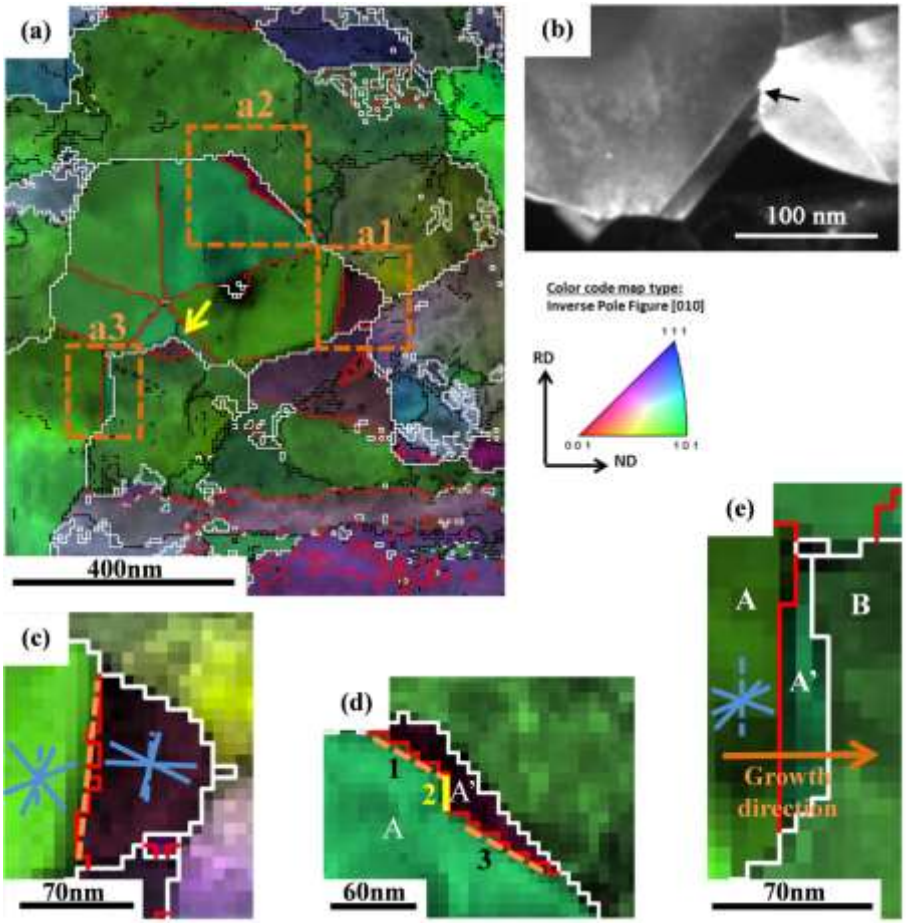

Fig. 5 Maps of grain orientations obtained by TEM with the ACOM system (IQ+IPF, color code for an inverse pole figure [010]), for sample A after annealing at 700°C for 6 min. (a) Several grains show the presence of twins. A five-fold twin occurs in the central grain. (b) Bright field image of the five-fold twin showing the sub-boundary (white arrow), indicated by a yellow arrow in Fig. 5a. The three regions delimited by squares a1, a2 and a3 are enlarged in (c) (d) and (e) respectively. Red lines figure Σ3 GBs, white lines High Angle GBs other than twins and black lines Low Angle GBs (LAGBs). The blue lines show the traces of 4 {111} plane traces in each grain. The blue dotted lines show the trace of the common twin plane on each side of the twin, and the orange arrow shows the growth direction deduced from the curvature of the migrating boundary. The yellow arrow indicates the presence of a sub-grain in the five-fold twin

The mechanisms proposed for formation of five-fold twins as reviewed in [29] distinguish cyclic twinning operation due to either a mistacking of atoms or deformation twinning as an accommodation process of plane strains in growing thin films [29]. However the mechanism of five-fold growth in polycrystalline nanosized metals has not been evidenced experimentally. MD simulations of grain growth in nanocrystalline copper at zero external pressure, and high temperature reveal that five-fold twins occur during annealing [30]. Five-fold twins result from local shear stresses at GBs and the proposed mechanism is a sequential emission of partial dislocations as reported in [31]. This work demonstrates that very high stresses are present and originate from the small grain size in the absence of any applied stress.

3.3 Influence of deformation on annealing twins

The influence of deformation on annealing twin formation was investigated after complete recrystallization at 900°C on samples that underwent increasing levels of deformation. The recrystallization was finished after 4 min thus the recovery process was considered to be negligible [16].

The densities of Σ3 (including Σ3coh and Σ3incoh), and Σ9 GBs were analyzed in these completely recrystallized samples. For each GB type, the density is defined as its total length divided by the analysis surface [16, 32]. The total lengths of Σ3, Σ3coh and Σ9 obtained from OIM^{TM} analysis are shown in Fig. 6 as a function of deformation prior to the annealing. The Σ3coh density increases with increasing deformation, except for the sample B after stronger deformation (ε=1.86). This exception is interpreted by the very small average grain size after complete recrystallization (grain size = 2.2 μm). The length of some Σ3coh boundary is very short; it does not contain enough pixels by segment, and can be hardly recognized as Σ3coh by OIM^{TM} analysis [33]. However, with regard to the density of total Σ3 GBs, it always increases with increasing deformation. All these results indicate that a higher stored energy before recrystallization favors the formation of twin boundaries.

Besides, the Σ3incoh and Σ9 GBs are an outcome from Σ3coh formation. The density of Σ3incoh GBs therefore increases with deformation. However, the Σ9 GB density is almost identical whatever the deformation; as it is very low, a possible small evolution versus the deformation is difficult to detect.

The stored energy has also an influence on the velocity of GB migration during recrystallization. Therefore, the twin formation may be related to the velocity of GB migration. One can also find the densities of these GBs are always greater in sample B than in A. It is mentioned above that a local deformation is formed around the particles. During the subsequent annealing, this local deformation contributes to increase locally the GB migration velocity that favors the twin formation. Such an effect has already been found in another Ni-based alloy [32].

4 Discussion

4.1 Active twinning system

In Fig. 5e, the blue lines in the grain A show the 4 {111} plane traces and it can be found that the coherent twin AA' matches one of these planes (dotted one) whose normal direction is close to the growth direction. This direction is deduced from the

curvature of the migrating boundary. So the formation of coherent twins depends on the growth direction as already proposed by Gleiter [3] and this can explain the formation of parallel twins in some recrystallized grains like those shown in Fig. 2d.

In Fig. 7, the new grain formed by PSN grows simultaneously towards two different directions (respectively indicated by orange arrows in area a1 and a2). The coherent twins are perpendicular to the growth direction. This feature occurs in both materials whatever the involved mechanism (SIBM and PSN).

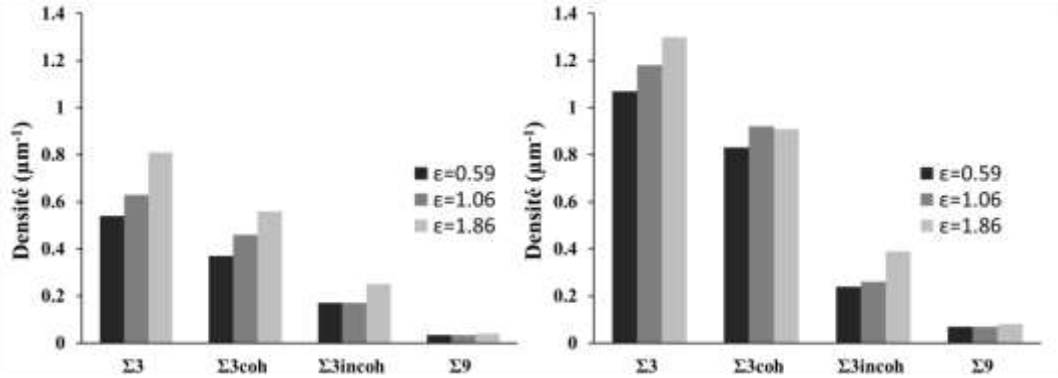

Fig. 6 Densities of Σ3 (including Σ3coh and Σ3incoh), Σ3coh, Σ3incoh and Σ9 GBs after different strain amount followed by the complete recrystallization, respectively for (a) sample A et (b) sample B

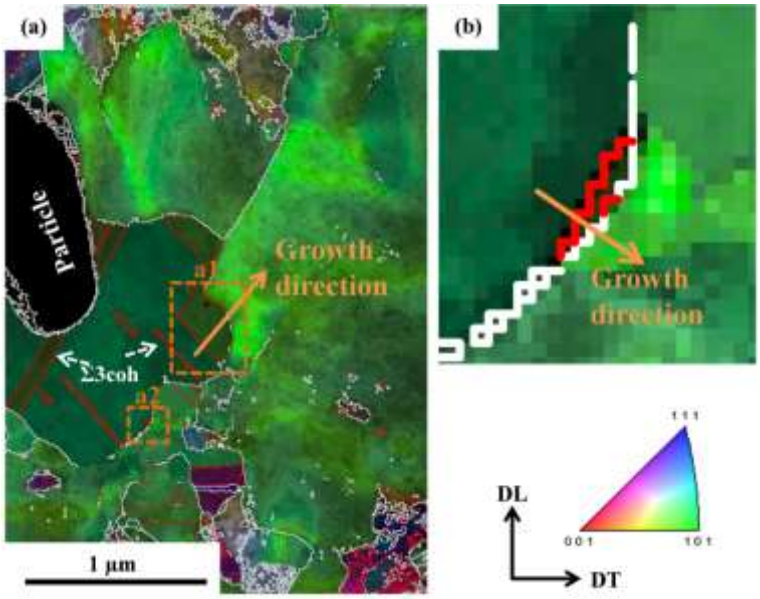

Fig. 7 Maps of grain orientations obtained by TEM with the ACOM system (IQ+IPF, color code for an inverse pole figure [010]), for sample B after annealing at 700°C for 6 min. (a) a new grain close to a W particle display several twins. The area a2 is enlarged in (b). Red and white lines show Σ3 GBs and High Angle GBs (HAGBs) respectively. The orange arrow shows the growth direction deduced from the curvature of the migrating boundary

4.2 Energy variation during twin formation

The stored energy of the different grains including twinned grains has been estimated from the determination of local misorientations, using the Kernel Average Misorientation (KAM) calculation [34-35].

The KAM map points out the local misorientation (Fig. 8). The pixel of the ACOM image is coming from a square grid, and the kernel size is chosen considering the 3rd neighboring pixels (or 30 nm). If the misorientation of any 3rd neighboring pixel with respect to the considered pixel is larger than 15°, this pixel will be considered as belonging to another crystal. Every pixel is then color coded as function of its KAM value and twins are indicated by white arrows. The average KAM and standard deviation (StD) for some grains and twinned parts of Fig. 8 are shown in table 3. The misorientation values are small, due to the small kernel size. For some grains, a high StD value reflects an heterogeneous distribution of the deformation. Most importantly, from table 3, these local misorientations are lower in some twinned parts (T1-T2, T6-T7) than in their parent grains (G1-G2, G12). Thus it is shown experimentally for the first time that the twinning process is associated to a further decrease in the stored energy during recrystallization. This can explain why the migration of old GBs happened when the recovery of the parent grains was not finished and the twins are formed during this migration.

In the following, the respective role of interfacial energy and stored energy on twinning is discussed.

Both growth accident [1], GB dissociation and nucleation of twins by stacking fault emission [4] theories involve a global decrease in the interfacial energy ΔEG. This applies for special cases where the newly created GB has a low energy [4]. In the general case, the decrease in the deformation level (stored energy) ΔES should be also considered. Therefore, the variation of total energy ΔE during twinning is described by Eq. 1, and the criterion of twinning formation is $\Delta E < 0$.

$$\Delta E = \Delta EG + \Delta ES \quad (1)$$

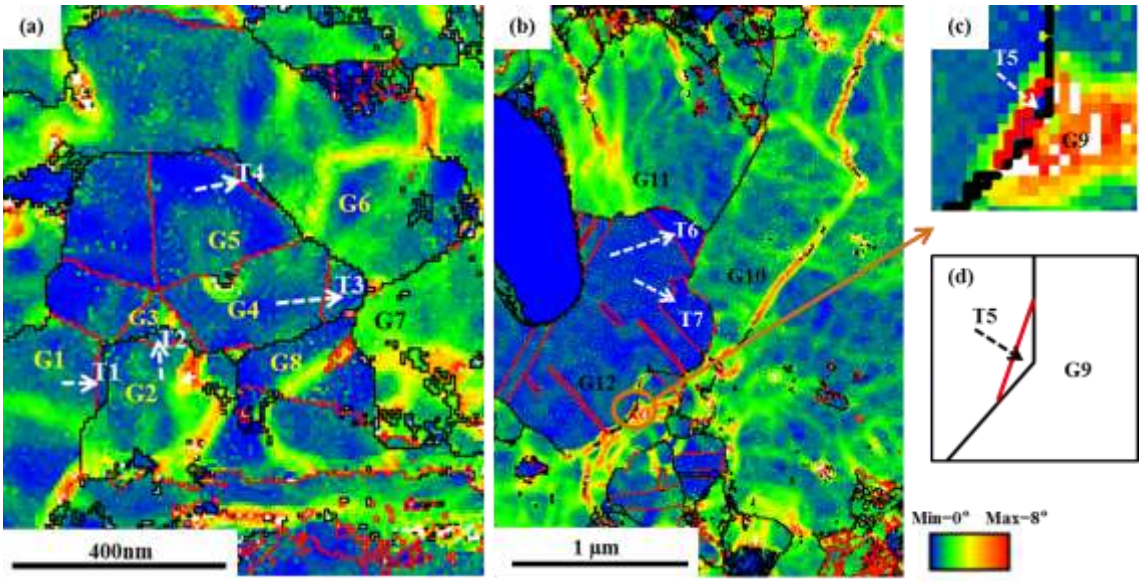

Fig. 8 (a) KAM map of Fig. 5a, and (b) KAM map of Fig. 7a. All the pixels are color coded to show the local misorientation (black and red lines show respectively the HAGBs and Σ3 GBs). The region circled in orange in (b) is enlarged in (c) and simplified in (d)

Table 3 Average KAM values for some twin parts and grains presented in figures 8 (the value of T5

is not calculated, because it corresponds to a very small area)

Twin	Average KAM (°)	StD (°)	Growing grain (Parent grain)	Average KAM (°)	StD (°)	Shrinking grain	Average KAM (°)	StD (°)
T1	**0.7**	**0.4**	**G1**	**1.2**	**1.1**	**G2**	**1.8**	**1.5**
T2	**0.6**	**0.4**	**G2**	**1.8**	**1.5**	**G3**	**1.2**	**1.7**
T3	**0.6**	**0.3**	**G4**	**0.8**	**0.5**	**G6** **G7** **G8**	**1.3** **2.6** **0.9**	**0.8** **1.2** **0.9**
T4	**0.6**	**0.3**	**G5**	**0.5**	**0.4**	**G6**	**1.3**	**0.8**
T5	**/**	**/**	**G12**	**0.5**	**0.5**	**G9**	**2.9**	**2.1**
T6	**0.1**	**0.1**	**G12**	**0.5**	**0.5**	**G11**	**1.5**	**0.9**
T7	**0.2**	**0.2**	**G12**	**0.5**	**0.5**	**G10**	**1.3**	**0.6**

In the example shown in Fig. 5e, the GB AB has migrated and a twin boundary AA' is formed. The variation in interfacial energy due to the twin formation is written as equation (2).

$$\Delta EG=(\gamma_{AA'}\times S_{AA'}+\gamma_{A'B}\times S_{A'B})-\gamma_{AB}\times S_{AB} \quad (2)$$

Where S is the GB surface and γ is the interfacial energy. The grain boundary energy $\gamma_{AA'}$ for coherent twin is almost zero. Moreover, at the onset of twinning, the surface of newly formed interface A'B is almost equal to that of AB. Also GBs AB and A'B are high angle GBs with 57° and 19° misorientation. Even though the grain boundary energy depends on its structure, it is always considered as high and similar for all high angle GBs (misorientation angle greater than 15°, including Σ9) except for the Σ3 and Σ11 {113} symmetrical ones [5-6, 21, 36-37]. Energy computation of a large set of GBs confirm the low energy of these GBs and those vicinal to these orientations [38]. Twist <111> GBs and in a less extent twist <100> GBs also display a low energy. Using an approach that determines the geometrical probabilities for finding GBs lying close to specific orientations in a polycristalline aggregate [39], the proportion of GBs with a misorientation axis deviated by 2° from <100> and <111> is 1.5%. If the GB plane is restrained to {100} and {111} planes respectively, the proportion of such twist GBs is negligible. For most other high angle GBs, the energy varies from 1 to 1.4 J/m^2.

Thus it can be assumed that the variation of grain boundary energy ΔEG during twinning is almost negligible. Then ΔE includes only the variation of stored energy before and after twinning, ΔES (Eqs. 3 and 4):

$$\Delta ES = [\Delta G_{SA}\times V_A + \Delta G_{SA'}\times V_{A'} + \Delta G_{SB}(V_B-V_{A'})]-(\Delta G_{SA}\times V_A + \Delta G_{SB}\times V_B) \quad (3)$$

Then:

$$\Delta ES = (\Delta G_{SA'} - \Delta G_{SB})V_{A'} \quad (4)$$

Where ΔG is the stored energy per unit volume, V_A and V_B are the volumes of grains A and B before twinning, and $V_{A'}$ is the volume of the twin part A'. As ΔG_{SB} is larger than $\Delta G_{SA'}$, ΔES is negative as expected. Moreover it is larger in absolute value than its value obtained in case of GB migration without twinning, $\Delta ES=(\Delta G_{SA}-\Delta G_{SB})V_{A'}$. Local misorientation variation is lower in the twinned part A' that presents KAM values lower than 1°, and thus is considered as a fully recrystallized area with null stored energy (T1 in Fig. 8a). The grains A and B with KAM values greater than 1° can be considered as zones with non-null stored

energy (G1 and G2 in Fig. 8a).

In the absence of recovery, which should decrease rapidly the stored energy, the ΔG_{SB} value for the deformed area depends on the strain amount ε prior to heat treatment (Eq. 5). C is a constant.

$$\Delta G_{SB} = - C \times \varepsilon \times V_A, \quad (5)$$

As the twin area corresponds to a well recrystallized area, the energy variation ΔES reduces to ΔG_{SB}. In summary, a higher strain before annealing leads to a higher decrease in stored energy by twinning, and this favors twin formation. This hypothesis is in agreement with statistical results of Fig. 6. The influence of stored energy or prior deformation on twin formation is emphasized by the Fig. 9 that shows the number of twin boundaries per grain as a function of grain size, after complete recrystallization of sample A [16]. Before the recrystallization treatments, this sample was deformed up to different strain levels. The number of twin boundaries increases with the grain size as expected. It is worth noting that for a given grain size, a higher prior deformation induces a higher number of twins formed at the onset of recrystallization.

4.3 Mechanism of annealing twins

The mechanism of twining is still controversial. Depending on the authors, it could result from a growth accident or be produced by emission of partial dislocations from the migrating GBs.

The annealing twins can be easily developed by higher strain amount that favors the higher velocity of GB migration during annealing. Conversely, it was also found that twin formation happened to restart the restrained grain growth or GB migration, during annealing at low temperature [13]. Twinning is an accommodation mechanism that favors the dislocation slip and GB migration to induce stress relaxation. During migration in the deformed matrix, GBs absorb lattice dislocations that give rise to a non-equilibrium state. For higher migration rate, more dislocations will be absorbed, and their accommodation in the GB will be more difficult. These arguments, associated with the occurrence in the present partially recrystallized nickel alloys of microtwins with partial dislocations support the role of emission of partial dislocations from moving GBs. Moreover, this mechanism has been shown to occur in MD simulations [10].

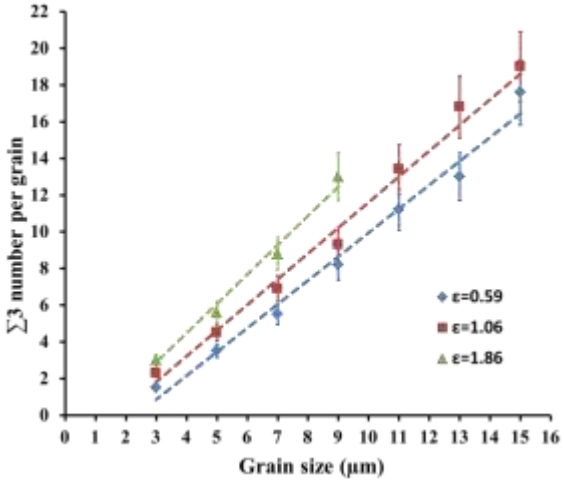

Fig. 9 Number of twin boundaries (including Σ3coh and Σ3incoh ones) as a function of grain size after complete recrystallization of sample A. The three curves correspond to three different strain levels, 0.59, 1.06 and 1.86 undergone by the sample before annealing treatments

5 Conclusions

It is concluded that twinning depends on the stored energy that is typically the driving force for nucleation and grain growth during the primary recrystallization. A higher stored energy gradient favors the twin formation because of the higher GB migration rate. Moreover, the presence of second phase allows the local deformation around the particles that increases locally the GB migration. This favors also the twin formation.

As a matter of fact, a decrease in stored

energy in twinned parts is directly emphasized from local misorientation measurements in the present experiments. Additionally, twinning plane is related to the direction of GB migration or grain growth, whatever the recrystallization mechanism (SIBM or PSN). When one of the 4 <111> axes of a grain is very close to its growth direction, a coherent twin is formed with this axis as the common axis. This condition explains the twin orientation selection among the four possible variants.

Acknowledgement

The authors wish to thank Isabelle DROUELLE, Denis SOLAS and Thierry AUGER for fruitful discussions, and acknowledge the support of Aubert & Duval for providing the material.

References

[1] Fullman RL and Fisher JC (1951) Formation of annealing twins during grain growth, J Appl Phys 22: 1350-1355.

[2] Ashby MF and Harper E (1967) Harvard Rept. Sept, Harvard University, Cambridge, MA.

[3] Gleiter H (1969) The formation of annealing twins, Acta Metall 17: 1421-1428.

[4] Meyers MA and Murr LE (1978) A model for the formation of annealing twins in fcc metals and alloys, Acta Metall 26: 951-962.

[5] Sutton AP, Balluffi RW (1995) Interfaces in Crystalline Materials. Clarendon Press, Oxford.

[6] Priester L (2013) Grain Boundaries: From Theory to Engineering. Springer, Dordrecht.

[7] Mahajan S, Pande CS, Imam MA, Rath BB(1997) Formation of annealing twins in fcc crystals, Acta Mater 45: 2633-2638.

[8] Rath BB, Imam MA, Pande CS (2000) Nucleation and growth of twin interfaces in fcc metals and alloys, Mater. Phys. Mech 1: 61-66.

[9] Dash S, Brown N (1963) An investigation of the origin and growth of annealing twins, Acta Metall 11: 1067-1075.

[10] Farkas D, Bringa E, Caro A (2007) Annealing twins in nanocrystalline fcc metals: A molecular dynamics simulation, Phys. Rev. B 75: 184111 (1-5).

[11] Huang P, Dai GQ, Wang F, Xu KW, Li YH (2009) Fivefold annealing twin in nanocrystalline Cu, Appl. Phys. Lett 95: 203101 (1-3).

[12] Pande CS, Imam MA, Rath BB (1990) Study of annealing twins in fcc metals and alloys, Metal. Trans A 21: 2891-2896.

[13] Field DP, Bradford LT, Nowell MM, Lillo TM (2007) The role of annealing twins during recrystallization of Cu, Acta Mater 55: 4233-4241.

[14] Bair JL, Hatch SL, Field DP (2014) Formation of annealing twin boundaries in nickel, Scripta Mater 81: 52-55.

[15] Jones AR (1981) Annealing twinning and the nucleation of recrystallization at grain boundaries, J. Mater. Sci 16: 1374-1380.

[16] Wang W, Brisset F, Helbert AL, Solas D, Drouelle I, Mathon MH, Baudin T (2014) Influence of stored energy on twin formation during primary recrystallization, Mat. Sci. Eng. A 589: 112-118.

[17] Jin Y, Bernacki M, Rohrer GS, Rollett AD, Lin B, Bozzolo N (2013) Formation of annealing twins during recrystallization and grain growth in 304L austenitic stainless steel, Mater. Sci. Forum 753: 113-116.

[18] Jin Y, Lin B, Bernacki M, Rohrer GS, Rollett AD, Bozzolo N (2014) Annealing twin development during recrystallization and grain growth in pure nickel, Mat. Sci. Eng. A 597: 295-303.

[19] Zhao H, Weatherly GC (1990) The formation of multi-domain precipitates in a Ni-W alloy, Acta Metall. Mater 38: 2253-2260.

[20] Rauch EF, Veron M (2005) Coupled microstructural observations and local texture measurements with an automated

crystallographic orientation mapping tool attached to a TEM, Materialwiss. Werkstofftech 36: 552-556.
[21] Humphreys FJ, Hatherly M (2004) Recrystallization and related annealing phenomena 2nd edn. Elsevier, Oxford.
[22] Beck PA, Sperry PR (1950) Strain induced grain boundary migration in purity aluminum, J Appl. Phys 21: 150-152.
[23] Penelle R, Baudin T (2010) Primary recrystallization of Invar, Fe-36%Ni alloy: origin and development of the cubic texture, Adv. Eng. Mater 12: 1047-1052.
[24] Cahn JW, Mishin Y (2009) Recrystallization initiated by low-temperature grain boundary motion coupled to stress, Int. J. Mat. Res 100: 510-515.
[25] Randle V (2004) Twinning-related grain boundary engineering, Acta Mater 52: 4067-4081.
[26] Melmed AJ, Hayward DO (1959) On the occurrence of fivefold rotational symmetry in metal whiskers, J Chem Phys 31: 545-546.
[27] Marks LD (1994) Experimental studies of small particle structures, Rep. Prog. Phys 57: 603-649.
[28] An XH, Lin QY, Wu SD, Zhang ZF, Figueiredo RB, Gao N, Langdon TG (2011) Formation of fivefold deformation twins in an ultrafine-grained copper alloy processed by high-pressure torsion, Scripta Mater 64: 249-252.
[29] Hofmeister H (2004) Fivefold twined nanoparticles. In: Nalwa HS (eds) Encyclopedia of Nanoscience and Nanotechnology 3th volume. American Scientific Publishers, California, pp.431-452.
[30] Bringa EM, Farkas D, Caro A, Wang YM, McNaney J, Smith R (2008) Fivefold twin formation during annealing of nanocrystalline Cu, Scripta Mater 59: 1267-1270.
[31] Zhu YT, Liao XZ, Valiev RZ (2005) Formation mechanism of fivefold deformation twins in nanocrystalline face-centred-cubic metals, Appl. Phys. Lett 86: 103112 (1-3).
[32] Bozzolo N, Souaï N, Logé RE (2012) Evolution of microstructure and twin density during thermomechanical processing in a γ-γ' nickel-based superalloy, Acta Mater 60: 5056-5066.
[33] Wright SI, Larsen RJ (2002) Extracting twins from orientation imaging microscopy scan data, J Microsc 205: 245-252.
[34] Brewer LN, Field DP, Merriman CC (2009) Mapping and assessing plastic deformation using EBSD. In: Schwartz AJ, Kumar M, Adams BL, Field DP (eds) Electron Backscatter Diffraction in Materials Science 2nd edn. Springer, New York, 2009, pp.251-262.
[35] Calcagnotto M, Ponge D, Demir E, Raabe D (2010) Orientation gradients and geometrically necessary dislocations in ultrafine grained dual-phase steels studied by 2D and 3D EBSD, Mat. Sci. Eng. A 527: 2738-2746.
[36] Volovitch P, Baudin T, Penelle R, Caleyo F, Barrallier L (2007) Role of recovery in the recrystallization simulation application to a cold rolled IF-Ti steel and a cold drawn copper wire, Mater. Sci. Forum 550: 453-458.
[37] Duparc OH, Couzinié JP, Thibault-Pénisson J, Lartigue-Korinek S, Décamps B, Priester L (2007) Atomic structures of symmetraical and asymmetrical facets in a near Σ=9{221} tilt grain boundary in copper, Acta Mater 55: 1791-1800.
[38] Olmsted DL, Foiles SM, Holm EA (2009) Survey of computed grain boundary properties in face-centered cubic metals: I. Grain boundary energy, Acta Mater 57: 3694-3703.
[39] Warrington DH, Boon M (1975) Ordered structures in random grain boundaries; some geometrical probabilities, Acta Metall 23: 599-607.